Structural, Optical and Electrical Properties of Cu doped ZnO Thin Films Grown by RF Magnetron Sputtering: Application to Solar Photocatalysis

Bilel Khalfallah (bilel.khalfallah@enit.utm.tn)
university of Tunis El Manar https://orcid.org/0000-0002-1979-9137
I. Riahi
tunis el manar university
F. Chaabouni
Tunis El Manar University

Research Article

Keywords: ZnO thin films, Cu doping, RF magnetron sputtering, Powder target, Optoelectrical properties, Photocatalytic activity

Posted Date: February 19th, 2021

DOI: https://doi.org/10.21203/rs.3.rs-211058/v1

Version of Record: A version of this preprint was published at Optical and Quantum Electronics on April 23rd, 2021. See the published version at https://doi.org/10.1007/s11082-021-02861-8.

Effect of Cu Doping on the Structural, Optical and Electrical Properties of ZnO Thin Films Grown by RF magnetron sputtering: Application to solar photocatalysis

B. Khalfallah*, I. Riahi, F. Chaabouni

University of Tunis El Manar-Laboratory of photovoltaic Semiconductors Materials, BP 37, Le belvédère 1002-Tunis, Tunisia

E-mail address*: bilel.khalfallah@enit.utm.tn

Abstract

RF sputtered undoped and Cu doped ZnO (CZO) thin films were deposited on unheated glass substrates using a mixed Cu_2O and ZnO powders target at different Cu concentrations of 0, 1, 2, 3 and 4 wt.%. The effects of copper concentration on the structural, electrical, optical and photocatalytic properties of CZO films have been studied. From XRD and Raman spectroscopy studies, it was found that the deposited films were polycrystalline with a predominant hexagonal wurtzite structure along the c-axis perpendicular to the substrate surface. The presence of multiple interference fringes in the transmittance and reflectance spectra shows the good homogeneity of the films. All the films are highly transparent with transparency reaching 80% indicating the possibility to use these films as an optical window. The absorption tail gradually shifted towards a higher wavelength side, which resulted in the decrease of bandgap energy from 3.35 to 3.26 eV. All the sputtered films are highly conductive with a conductivity reaching 10^4 $S.cm^{-1}$.The effect of Cu-doping on the photocatalytic activity of ZnO thin films for the degradation of methylene blue (MB) dye was studied under sunlight irradiation and the results showed that the Cudoping provokes appreciable degradation of MB and reached a maximum for the 1 wt.% Cu doped ZnO film.

Keywords: ZnO thin films; Cu doping; RF magnetron sputtering; Powder target; Optoelectrical properties; Photocatalytic activity

1. Introduction

Over the past three decades, oxide semiconductor thin films, and particularly zinc oxide have been the subject of a great deal of research[1-5]. Zinc Oxide (ZnO) is a semiconductor with interesting electrical and optical properties. The importance of its binding exciton energy (60 meV), and the width of its bandgap (3.37 eV), makes it a good candidate for applications in different technological sectors, notably in optoelectronics as transparent electrodes and ultraviolet detectors or laser diode emitting in blue or ultraviolet, in photovoltaic for production of solar cells, in piezoelectric for mechanical detectors, in acoustic wave devices and environmental applications [6-10]. Doping of suitable elements in ZnO shows different functions and improved, in particular, its electrical and optical properties, which facilitate the development of many electronic and optoelectronic devices [11-13]. It is expected that doping can enhance the diversity of applications of this oxide. Among the doping impurity elements, Copper Cu is an attractive dopant due to its high conductivity and being relatively abundant on the Earth's crust. Also, doping with Cu helps in obtaining p-type ZnO. Photocatalytic properties of ZnO can be tailored by doping with foreign elements in ZnO such as Cu [14], Fe [15], Ni [16], Co [17], and N [18]. Among these doping elements, copper Cu is one of the doping metals of interest because it is widely used as a catalyst for many reactions and can

have a significant influence on the photocatalytic performance of materials. Different technological processes can be used to deposit ZnO thin films, including Spray pyrolysis, Sol-Gel, Laser Ablation and Magnetron Sputtering [19-22].

In this study, our research efforts are focused on the investigation of the effect of Cu doping on the structural, optical, electrical and photocatalytic efficiency of ZnO films deposited on a glass substrate at room temperature by a simple and inexpensive RF sputtering technique using raw powder targets as an alternative to the typical sputter target, where a relatively expensive ZnO sintered target was used. The photocatalytic activities were tested for the degradation of methylene blue (BM) under sunlight irradiations. All obtained results are correlated, and the enhanced photocatalytic activity is interpreted based on structural, optical and electrical investigations.

2. Experimental details

Undoped and Cu-doped ZnO (CZO) thin films were deposited at room temperature onto the glass substrates by RF magnetron sputtering technique using a raw powder target. The 99.99% pure Cu2O and ZnO powders with particle sizes in the range of 100 nm to 1 µm were mixed with the mass ratio of 1, 2, 3 and 4 wt.% and blended in a rotatable drum. The blended powders were spread onto a copper plate and lightly tamped down to produce a uniform thickness and surface to target distance. No further processes (such as sintering) were involved in target production. The chamber was evacuated to a base pressure lower than 10^{-4} Pa and then backfilled with argon gas to a pressure of 0.6 Pa. The sodium glass slides used as substrates were RF sputter cleaned in situ at 200 W for 15 min before deposition. The substrates were rotated (15 rd/mn) and the target–substrate separation was fixed at 65 mm.

The crystalline structure was analyzed by X-ray diffraction using a Siemens D500 diffractometer with monochromatic CuK_α radiation ($\lambda=1.54$ Å). On the other hand, Raman scattering experiments were carried out using a Renishaw micro-Raman system at room temperature. The optical properties of the deposited films were measured at normal incidence in the wavelength range from 300 to 1800 nm using a double-beam UV–VIS–NIR spectrophotometer (Shimadzu). The photoluminescence (PL) measurements were performed at room temperature using a He-Cd laser operating at 325 nm. Finally, electrical resistivity, Hall mobility and carrier concentration were measured at room temperature by a Hall measurement system with the Van der Pauw method.

3. Results and discussion

3.1. X-ray diffraction and Raman scattering study

The highly crystalline, c-axis oriented and columnar structured Cu-doped ZnO thin film was confirmed by X-ray diffraction as shown in Fig. 1. The XRD patterns of the CZO films show mainly a (002) and (004) diffraction lines of ZnO hexagonal wurtzite structure (JCPDS File No: 00-036-1451), i.e., indicating that all films have the c-axis orientation perpendicular to the substrate, which has been confirmed by a previous study [23]. No other phases for Cu and their oxides can be detected in the films, indicating that Cu doping does not alter the hexagonal structure and confirm the uniformity of Cu-doped ZnO thin films. It is noted that increasing the Cu-doping concentration reduced the intensity of the (002)peak, suggesting that Cu-doping can degrade the (002) preferential orientation of CZO thin films. This can be explained by the fact that the additional Cu ions, apart from replacing the Zn ions, may occupy the interstitial positions in the ZnO lattice where they form neutral defects and become ineffective as

dopant impurities. The crystalline size of CZO thin films was evaluated using the full-width at half-maximum (FWHM) of the (002)-peak according to Scherrer's equation [24]:

$$D = \frac{0.9\lambda}{\beta \cos\theta} \tag{1}$$

where λ (1.541 Å) is the wavelength of *Cu* K_α radiation,θ is the Bragg angle, and β is the half-width at half maximum (HWHM) of the (002) peak. The values of average crystallite size are summarized in Table 1.Fig.1 (c) shows that the crystalline size of the CZO thin films decreased with increasing Cu concentration from 33 nm to 22 nm. This finding indicated that Cu doping deteriorated the crystal quality of the ZnO thin films. Moreover, Fig. 1 (b) shows that the (002) peak slightly shifted toward lower angles with increased Cu concentration, which resulted in an increase in the lattice parameter according to Bragg's formula [24]:

$$d_{hkl}{}^2 = \left(\frac{4\left(h^2 + k^2 + hk\right)}{3a^2} + \frac{l^2}{c^2} \right) \tag{2}$$

where d_{hkl} denotes the crystalline plane distance of (*h, k, l*) indices. Since the Cu^{2+} (0,72 Å) ionic radius is smaller than the Zn^{2+} ion (0,074 Å) [25], and hence the substitution of Cu in the Zn site increases the lattice parameter as showing in Table 1.

To evaluate the effect of Cu-doping on vibrational properties, room temperature Raman scattering analysis ranging from 100 to 1000 cm^{-1} was performed (Fig. 2). The wurtzite ZnO belongs to the space group of C_{6v}, with six active Raman modes of E_{2L}+E_{2H}+A_{1T}+A_{1L}+E_{1T}+E_{1L}[26]. As showing in Fig. 2, a specific peak corresponding to the E_2 high-frequency E_2(high) branch at wave number around 439 $cm^{-1}$was observed in the Raman spectrum of the undoped and Cu doped ZnO sample. As the Cu concentration increased, the E_2(high) mode was gradually decreased and broadened. From the previous works, the E_2(high) phonon mode is typically related to the crystalline quality, phase orientation, and strain present in the ZnO matrix [27–29]. So, the decrease of E_2(high) peak intensity as the Cu concentration increased was attributed to the deterioration of the crystalline structure of ZnO thin film, as confirmed from the degradation of the c-axis growth orientation discussed in the XRD analysis. In addition to the E_2 (high) mode, A_1(TO) and A_1(LO) modes were observed at wavenumbers around 380 and 580 cm^{-1}in the Raman spectra of all samples. The A1(LO) and A_1(TO) modes are reported to be linked to the abundant shallow donor defects such as oxygen vacancy (V_O) or interstitial Zn (Zn_i) in ZnO material [28]. On the other hand, the relative intensity of A_1(LO) and A_1(TO) phonon modes decreased as Cu doping concentration increase from 0 to 4 wt.%, which indicates that some defect concentration related to deep level emission might have been decreased. The Raman mode observed at wave number at about 275 cm^{-1} corresponds to B_1(low) phonon mode frequency and it's observed in all samples. From previous theoretical and experimental studies, this Raman mode was attributed to the localized vibration of Zn atoms, where parts of their first nearest neighbor O atoms are replaced by Cu atoms in the ZnO lattice [30]. Also, the presence of this mode may be due to Raman diffusion indicating the presence of the structural disorder in all deposited films. So, photoluminescence spectra analysis was performed to confirm these results and to understand the effect of Cu doping on the optoelectrical properties.

3.2. UV–Vis–NIR and Photoluminescence study

Fig. 3 shows the optical transmittance and reflectance spectra of undoped and Cu doped ZnO thin films over a spectral range of 300-1800 nm. The fringes associated with interference effects confirm the optical homogeneity and the excellent surface quality of the deposited films. All prepared films exhibit good transparency in the visible range (> 80%) and a sharp fundamental absorption edge around a wavelength of 360 nm, indicating that these materials are suitable for use as a transparent electrode. The absorption edge of direct bandgap semiconductor thin films can be analyzed to estimate the optical band gap by using the following equation [31, 32]:

$$(\alpha h\nu)^2 = A(h\nu - E_g^{\ opt}) \tag{3}$$

where α is the absorption coefficient, $h\nu$ is the photon energy, A is a constant and E_g is the optical bandgap energy. Fig. 4 shows the plot of $(\alpha h\nu)^2$ versus $h\nu$ of undoped and Cu doped ZnO thin films deposited at various Cu concentrations. The straight-line portion of the curve, when extrapolated to zero, gives the optical band gap E_g. The bandgap energy values E_g for the deposited films are summarized in Table 1. Remarkably, the bandgap energy values of CZO thin films decreased with increasing Cu concentrations. According to a previous report [32], the decrease in the bandgap energy may be due to thesp–d spin-exchange interactions between the band electrons and the localized d electrons of the metal ion (Zn) substituting the Cu ion. Moreover, the difference in the electronegativity between Cu and Zn atoms may induce some defects resulting in a decrease of bandgap energy [33].

Room temperature photoluminescence (PL) measurements were carried out for a more detailed investigation of defects that existed in the Cu-doped ZnO films. The PL spectra of Cu-doped ZnO films have been recorded by using He-Cd laser at an excitation wavelength of 325 nm. Fig. 5 shows the deconvolution of PL spectra of undoped and Cu doped ZnO thin films at various Cu contents. From this deconvolution, it is seen that four emission peaks were observed at around 386 (3.21 eV), 415 (2.98 eV) 484 (2.56 eV) and 530 nm (2.33 eV) for all deposited samples and are in good agreement with previous reports [34]. A strong UV emission peak located at about 386 nm is related to a near band-edge transition of ZnO, namely, the recombination of the free excitons [35]. As shown in Fig.6, the UV emission peak shifted to a higher wavelength with increasing the Cu doping concentration. Indeed, ZnO is a kind of n-type semiconductor and Cu atom is a p-type dopant. So, this shift of the UV emission peak can be attributed to the sp–d spin-exchange interactions between the band electrons and the localized d electrons of the metal ion (Zn) substituting the Cu ion [32]. Amol R. et *al*. [36] reported also that the value of bandgap energy (E_g) should decrease after Cu doping into ZnO crystal lattice.PL results are in agreement with the UV-Vis spectroscopy studies and support the observation of a decrease in the bandgap energy on increasing Cu doping concentration. On the other hand, it was found that the progressive addition of Copper Cu reduces the absolute intensity of the observed UV emission peak. A similar result is also reported in Cu- doped ZnO films [37], N-doped ZnO films [38] and Ni-doped ZnO films [39] and can be ascribed to the density of free exciton in ZnO thin films affecting the intensity of ultraviolet emission[40]. The emissions observed in the visible region have previously been attributed to several defective states within bandgap energy, such as oxygen vacancy (V_O), zinc vacancy (V_{Zn}), oxygen interstitial (O_i) and zinc interstitial (Zn_i) [41]. In our study, the violet emission energy centered at 2.98 eV which may be assigned to the transition energy of Zn_i defect level to the valence band maxima. According to the theoretical calculation, P. S. Xu et *al*. have previously investigated the violet emission energy of the ZnO and found it to be correlated with the density of Zn_i defects [42]. Himanshi Gupta et *al*. reported that the

blue emission could be originated from the recombination of a delocalized electron in the conduction band with a hole in the singly ionized oxygen vacancies [43]. Based on the theoretical approach presented by Federico Gallino et *al.*the transition energy between the conduction band and the singly ionized V_O (+1/0) level was 2.52 *eV* [44]. Thus, we proposed that in our films, the blue emission can be ascribed to the singly ionized oxygen vacancies. The emission peak centered at about 2.33 eV is attributed to green luminescence and can be assigned to the transition from the defect level of neutral zinc interstitial Zn_i to the valance band maxima which is consistent with the results reported by L. T. Tseng et *al*. [45].

3.3 Hall effect Study

Hall measurements were performed in a Van der Pauw four-point configuration at room temperature and the corresponding results are listed in Table 2. From previous reports, Cu doping introduces an acceptor (Cu^+) level in ZnO at 0.45 eV above the valence band [46,47]. So, we can conclude from these reports that Cu may assume a valency of either +1 or +2 depending on its chemical environment. In our study, we found that all the deposited Cu doped ZnO films exhibit *n*-type conductivity. This result is surprising since the Cu ion is supposed to provide p-type ZnO. We can, therefore, think that the probable insertion in a substitution position of the Cu^+ion in the ZnO matrix is not sufficient to induce *p*-type conduction and (or) insertion is not total and that the non-inserted Cu ions are responsible for defects that can bring carriers of n-type conductivity. This behavior was observed by Chang Oh Kim et *al*. [48]in their study on the Cu doped ZnO thin films, but also in the ZnO thin films doped with Nitrogen N [49] or with Lithium Li [50].On the other hand, we can notice that the resistivity increases slightly with increasing the Cu doping concentrations while the carrier's mobility decreases slightly with increasing Cu doping concentration. This result is not surprising and supports the explanation given above. We have probably a competition between two opposite effects. The first is related to the insertion of the Cu ions into the ZnO matrix andis supposed to provide a *p*-type conductivity and therefore induce an increase in the resistivity of the films. The second effect is related to the increase in defects number due to the Cu ions not inserted in the ZnO matrix which can bring doping of *n*- type conductivity and therefore induce a decrease in the resistivity. This idea is supported by the decrease in the carrier's mobility which is intimately linked to the quality and purity of the deposited thin films. Indeed, the presence of ionized impurity and the existence of defects within the samples increases the probability of free carrier collisions. The vibration of the atoms of the crystal lattice around their equilibrium position is also an obstacle for free electrons. However, it should be borne in mind that the resistivity values before and after doping with Cu remain relatively low in the range of 10^{-4} - $10^{-2}\Omega.cm$ which shows that this system remains potentially interesting for photovoltaic applications.

3.4. Photocatalytic activity test

The photocatalytic activities of undoped and Cu doped ZnO thin films with different Cu concentrations were evaluated by monitoring the decomposition of methylene blue (MB) for 3 hours under sunlight irradiation. The analysis has been done in February, where the temperature was about 25 degrees. Undoped and Cu doped ZnO thin films with an area of 2x2 cm^2 were placed in a methylene blue solution (3 mg. l^{-1}) and this solution was stirred in the dark for 30 min to reach the adsorption-desorption equilibrium. Then, the MB decomposition testing was carried out by a UV-Visible spectrophotometer. Fig. 7 shows the absorption spectra of MB after solar irradiation for 3 hours for the 1 wt.% Cu doped ZnO film. It can be seen from these absorption spectra, the decrease in the

maximum absorption peak intensity is located at about 664 nm which indicates the degradation of the MB and the improvement of the photocatalytic activity of the films. For all the samples, they show the same tendency; that is to say, the MB concentration gradually decreased with the prolonging of irradiation time and the degradation efficiencies achieved 85%. To evaluate the influence of copper concentration on the photocatalytic properties of ZnO thin films, we have plotted the absorption spectra of MB after solar irradiation after 3 hours of undoped and Cu doped ZnO thin films at various Cu concentrations as showing in Fig. 8. Indeed, we can see an increase in the intensity of the absorption peak with the increase in Cu concentrations except for the 1 wt.% Cu doped ZnO film, confirmed by the low absorption peak intensity indicating its great photocatalytic activity compared to the other layers. This may be due to the high mobility and the important density of the charge carrier of this film. Also, we can explain this by the fact that at higher Cu doping concentration, the Cu atoms cannot occupy zinc lattice sites and they have a tendency to occupy interstitial sites where they form neutral defects that will serve as recombination centers for photogenerated electrons and can hind the electron-hole recombination affecting thus the photocatalytic activity [51].

The degradation efficiencies were evaluated by using the following relation [52, 53]:

$$Dye\ \% = ((A0 - A) / A0)*100 \quad (4)$$

Where A_0 is the initial ($t=0$) absorbance of MB and A is the absorbance at time t. Fig.9 shows the degradation efficiencies of MB dye versus irradiation time. The photocatalytic activity of the 1 wt.% Cu doped ZnO film is the highest and the degradation of MB is nearly up to 80% after 3 h of irradiation. So, we can notice that the ZnO films doped with a small amount of Cu could enhance the photocatalytic activity.

Fig. 10 shows the least fit curve of the logarithmic ratio of concentrations with time for the undoped and Cu doped films with different concentrations. The straight-line curve indicates that the rate of photo-degradation of MB dye obeys pseudo-first-order kinetics as stated by Langmuir-Hinshel Model [54]:

$$Ln\ (A_0/A) = k*t \quad (5)$$

where A is the absorption peak intensity at the desired irradiation time interval, A_0 the initial absorption intensity of MB dye, k the rate constant and t the irradiation time. The values of k are determined from the slope of the fitted curves and they are presented in Table3. The kinetic rate constant is estimated to be about 3.03 x 10^{-3} min^{-1} for MB in the absence of a photocatalyst. We can notice that the introduction of photocatalyst enhances the kinetic constant rate and improves the photocatalytic activity. The most important value of k is obtained for the 1 wt.% Cu doped ZnO film and is about 8.58 × 10^{-3} min^{-1} which confirms the best photocatalytic activity of this film.

Conclusions

In summary, we report ZnO thin films doped with varying Cu concentrations deposited by RF magnetron sputtering technique with recourse to a low-cost powder target. The structural analysis carried out by XRD suggested that the incorporation of Cu deteriorates the crystallinity of the host thin films. We have noticed from the UV-Vis analysis that all deposited films exhibit high transparency and increasing in Cu doping concentration leads to a decrease in the bandgap energy. PL spectra indicate that a high concentration of defects and impurities exist in the deposited films, which is in agreement with the results of Raman analysis. Finally, The photocatalytic activities of undoped and Cu doped ZnO thin films with different Cu concentrations were evaluated by monitoring the decomposition of methylene blue (MB) and we have concluded that the best photocatalytic activity was obtained for the 1 wt.% Cu doped ZnO film.

Declaration of interests

The authors declare that they have no known competing financial interests or personal relationships that could have appeared to influence the work reported in this paper.

References

[1] J.Kennedy, P.P.Murmu, E.Manikandan and S.Y.Lee, Journal of alloys and compounds **616** 614 (2014)

[2] John Kennedy, Grant V. M. Williams, Peter P. Murmu, and Ben J. Ruck, Physical review B **88** 214423 (2013)

[3] J. Kennedy, D. A. Carder, A. Markwitz and R. J. Reeves, Journal of Applied Physics **107** 103518 (2010)

[4] J.Kennedy, A.Markwitz, Z.Li, W.Gao, C.Kendrick, S.M.Durbin and R.Reevesd Current Applied Physics 6 (3), 495-498, 2006

[5] K. Kaviyarasu, Genene T. Mola, S. O. Oseni, K. Kanimozhi, C. Maria Magdalane, J. Kennedy and M. Maaza Journal of Materials Science: Materials in Electronics volume **30** 147 (2019)

[6] Linhua Xu, Wenjian Kuang, Zhanhui Liu, and Fenglin Xian, Physica B: Physics of Condensed Matter **583** 412010 (2020)

[7] Linhua Xu, Xiaoxiong Wang, Fenglin Xian, and Jing Su, Materials Research Bulletin **123** 110724 (2020)

[8] Weijia Yang, Junjie Liu, Mingquan Liu, Yanyi Liu, Nuoyuan Wang, Gengzhe Shen, Zhihao Liu, Xin He, Chi Zhang, Linshun Hu, and Yuechun Fu, Superlattices and Microstructures **136** 106291 (2019)

[9] Anna Kaźmierczak-Bałata, Jerzy Bodzenta, and Marek Guziewicz, Ultramicroscopy **210** 112923 (2020)

[10] Linhua Xu, Jing Su, Gaige Zheng, and Lei Zhang, Materials Science and Engineering: B **248** 114405 (2019)

[6] Toshihiro Miyata, Hiroki Tokunaga, Kyosuke Watanabe, Noriaki Ikenaga, and Tadatsugu Minami, Thin Solid Films **697** 137825 (2020)

[7] Qingqing Fan, Dongning Li, Junhong Li, and Chenghao Wang, Journal of Alloys and Compounds **829** 154483 (2020)

[8] Xiang Tao, Tan Dai Nguyen, Hao Jin, Ran Tao, Jingting Luo Xin Yang, Hamdi Torun, Jian Zhou, Shuyi Huang, Lin Shi, Des Gibson, Michael Cooke, Hejun Du, Shurong Dong, Jikui Luo, and Yong Qing Fu, Sensors and Actuators B: Chemical **299** 126991 (2019)

[9] Y.M.Hunge, A.A.Yadav, S.B.Kulkarni, and V.L.Mathe, Sensors and Actuators B: Chemical **274** 1 (2018)

[10] Mohamed Zayed, Ashour M.Ahmed, and Mohamed Shaban, International Journal of Hydrogen Energy **44** 17630 (2019)

[11] Y.Andolsi, and F.Chaabouni, Journal of Alloys and Compounds **818** 152739 (2020)

[12] Xu Li, Xinghua Zhu, Kangxin Jin, and Dingyu Yang, Optical Materials **100** 109657 (2020)

[13] H.Ali, A.M.Alsmadi, B.Salameh, M.Mathai, M.Shatnawi, N.M.A.Hadia, and E.M.M.Ibrahim, Journal of Alloys and Compounds **816** 152538 (2020)

[14] Nripasree Narayanan, and N.K.Deepak, Optik **158** 1313 (2018)

[15] D. Nithyaa Sree, S. Paul Mary Deborrah, C.Gopinathan, and S.S.R.Inbanathana, Applied Surface Science **494** 116 (2019)

[16] M.Sh.Abdel-wahab, Asim Jilani, I.S.Yahia, and Attieh A.Al-Ghamdi, Superlattices and Microstructures **94** 108 (2016)

[17] B.Poornaprakash, U.Chalapathi, K.Subramanyam, S.V. Prabhakar Vattikuti, Si-Hyun Parka, Ceramics International **46** 2931 (2020)

[18] Numan Salah, A. Hameed, M. Aslam, M.Sh. Abdel-wahab, Saeed S. Babkair, and F.S. Bahabri, Chemical Engineering Journal **291** 115 (2016)

[19] Said Benramachea, Achour Rahalb, and Boubaker Benhaoua, Optik **125** 663 (2014)

[20] M. Vishwasa, K. Narasimha Rao, A.R. Phani, K.V. Arjuna Gowda, and R.P.S. Chakradhar, Solid State Commun. **152** 324 (2012)

[21] Alex M. Ma, Manisha Gupta, Fatema Rezwana Chowdhury, Mei Shen, Kyle Bothe, Karthik Shankar, Ying Tsui, and Douglas W. Barlage Solid-State Electron. **76** 104 (2012)

[22] N.H. Al-Hardan, M.J. Abdullah, H. Ahmad, A. Abdul Aziz, and L.Y. Low, Solid-State Electron. **55** 59 (2011)

[23] Yong Liu, Haonan Liu,YangYu, QingWang,Yinglan Li and Zhi Wang, Materials Letters **143** 319 (2015)

[24] B. D. Cullity, and S. R. Stock, Elements of X-Ray Diffraction, Prentice-Hall, New York, 2001.

[25] Guo-Ju Chen, Sheng-Rui Jian, and Jenh-Yih Juang, Coatings **8** 266 (2018)

[26] C. Bundesmann, N. Ashkenov, M. Schubert, D. Spemann, T. Butz, E. M. Kaidashev, M. Lorenz, and M. Grundmann, APPLIED PHYSICS LETTERS **83** 1974 (2003)

[27] Seyda Horzum, Fadil Iyikanat, Ramazan Tugrul Senger, Cem Çelebi, Mohamed Sbeta, Abdullah Yildiz, and Tülay Serin, Journal of Molecular Structure **1180** 505 (2019)

[28] Naina Gautam, Himanshi Gupta, A. Kapoor, and Fouran Singh, Physica B: Condensed Matter **570** 13 (2019)

[29] Y.M. Hu, C.Y. Wang, S.S. Lee, T.C. Han, and W.Y. Chou, Thin Solid Films **519** 1272 (2010)

[30] Xiaming Zhu, Hui-Zhen Wu, Dong-Jiang Qiu, Zijian Yuan, Guofen Jin, Jinfang Kong, and Wenzhong Shen, Optics Communications **283** 2695 (2010)

[31] J. I. Pankove, Optical processes in semiconductors, Prentice-Hall, Englewood Cliffs, N.J., 1971.

[32] R. Elilarassi, and G. Chandrasekaran, J Mater Sci: Mater Electron **21** 1168 (2010)

[33] S. Muthukumaran, and R. Gopalakrishnan, Opt. Mater. **34** 1946 (2012)

[34] Adem Sreedhar, Jin Hyuk Kwon, Jonghoon Yi, Jong Su Kim, and Jin Seog Gwag, Materials Science in Semiconductor Processing **49** 8 (2016)

[35] L. Ouarez, A. Chelouche, T. Touam, R. Mahiou, D. Djouadi, and A. Potdevin, Journal of Luminescence **203** 222 (2018)

[36] Amol R. Nimbalkar, and Maruti G. Patil, Materials Science in Semiconductor Processing **71** 332 (2017)

[37] Qasem A. Drmosh, Saleem G. Rao, Zain H. Yamani, and Mohammed A. Gondal, Applied Surface Science **270** 104 (2013)

[38] Younggyu Kim, and Jae-Young Leem, Physica B **476** 71 (2015)

[39] A.A.M. Farag, M. Cavas, F. Yakuphanoglu, F.M. Amanullah, A.A.M. Faraga, M. Cavas, F. Yakuphanoglu, and F.M. Amanullah, Journal of Alloys and Compounds **509** 7900 (2011)

[40] Xiaolu Yan, Dan Hu, Hangshi Li, Linxiao Li, Xiaoyu Chong, and Yude Wang, Physica B **406** 3956 (2011)

[41] E. Hasabeldaim, O.M. Ntwaeaborwa, R.E. Kroon, and H.C. Swart, Journal of Molecular Structure 1192 **105** (2019)

[42] P. S. Xu, Y. M. Sun, C. S. Shi, F. Q. Xu and H. B. Pan, Nucl. Instrum. Methods Phys. Res., Sect. B **199** 286 (2003)

[43] Himanshi Gupta, Jitendra Singh, R. N. Dutt, Sunil Ojha, Soumen Kar, Ravi Kumar, V. R. Reddy, and Fouran Singh, Physical Chemistry Chemical Physics **21** 15019 (2019)

[44] Federico Gallino, Gianfranco Pacchioni, and Cristiana Di Valentin, The Journal Of Chemical Physics **133** 144512 (2010)

[45] L. T. Tseng, J. B. Yi, X. Y. Zhang, G. Z. Xing, H. M. Fan, T. S. Herng, X. Luo, and M. Ionescu, J. Ding, S. Li, AIP ADVANCES **4** 067117 (2014)

[46] Mohammad Suja, Sunayna B. Bashar, Muhammad M. Morshed, and Jianlin Liu, ACS Appl. Mater. Interfaces **7** 8894 (2015)

[47] D. C. Agarwal, U. B. Singh, Srashti Gupta, Rahul Singhal, P. K. Kulriya, Fouran Singh, A. Tripathi, Jitendra Singh, U. S. Joshi, and D. K. Avasthi, Scientific Reports **9** 6675 (2019)

[48] Chang Oh Kim, Sung Kim, Hyoung Taek Oh, Suk-Ho Choi, Yoon Shon, Sejoon Lee, Han Na Hwang, and Chan-Cuk Hwang, Physica B **405** 4678 (2010)

[49] Trilok Kumar Pathak, Vinod Kumar, H.C. Swart, and L.P. Purohit, Physica B: Condensed Matter **480** 31 (2016)

[50] DeYi Wang, Jian Zhou, and GuiZhen Liu, Journal of Alloys and Compounds **481** 802 (2009)

[51] A. Tabib, W. Bouslama, B. Sieber, A. Addad, H. Elhouichet, M. Ferid, and R. Boukherroub, Appl. Surf. Sci. **396** 1528 (2017)

[52] M. K. Nazarabad, and E. K. Goharshadi, Sol. Energy Mater. Sol. Cells **160** 484 (2017)

[53] R. Nasser, W. B. H. Othmen, H. Elhouichet, and M. Férid, Appl. Surf. Sci. **393** 486 (2017)

[54] K. Vasanth Kumar, K. Porkodi, and F. Rocha, Catalysis Communications **9** 82 (2008)

Table captions

Table 1 2Θ position, FWHM, crystallite size, lattice parameter and gap energy of the Cu doped ZnO films at various Cu contents

Table 2 Electrical resistivity (ρ), carrier concentration (n) and mobility (μ) of the Cu doped ZnO films at various Cu contents

Table 3 Variation of the kinetic constant with Cu contents.

Figure captions

Fig. 1 X-ray diffraction (XRD) patterns of the Cu doped ZnO thin films at various Cu contents **(a)**, the enlarging XRD patterns of the (002) plane peak **(b)**, the variation of FWHM and crystalline size at various Cu contents **(c)**.

Fig. 2 Raman scattering spectra of the Cu doped ZnO films at various Cu contents

Fig. 3 Optical transmission and reflectance of Cu-doped ZnO thin films at various CuContents

Fig. 4 The plots of $(ahv)^2$ against hv of Cu-doped ZnO thin films at various Cu contents

Fig. 5 Deconvoluted PL spectra of undoped and Cu-doped ZnO films at various Cu contents

Fig. 6 PL spectra of undoped and Cu-doped ZnO films at various Cu contents

Fig. 7 The absorption spectra of MB for the 1 wt.% Cu doped ZnO film

Fig. 8 Absorption spectra of MB after solar irradiation for 3 hours using the Cu doped ZnO thin films at various Cu contents.

Fig 9 The degradation efficiencies of MB dye versus irradiation time

Fig. 10 Photocatalytic degradation kinetics of MB for different photocatalytic systems as a

function of time under solar irradiation.

Table 1 2Θ position, FWHM, crystallite size, lattice parameter and gap energy of the Cu doped ZnO films at various Cu contents

Samples	**2Θ (°)**	**c** (Å)	**FWHM** (°)	**D (nm)**	**E_g (eV)**
Cu 0 wt.%	34.36	5,218	0.251	33	3.35
Cu 1wt.%	34.31	5,225	0.323	26	3.32
Cu 2 wt.%	34.22	5,239	0.342	24	3.28
Cu 3 wt.%	34.22	5,239	0.351	23	3.28
Cu 4 wt.%	34.21	5,240	0.371	22	3.26

Table 2 Electrical resistivity (ρ), carrier concentration (n) and mobility (μ) of the Cu doped ZnO films at various Cu contents

Samples	ρ (*10^{-3} Ω.cm)	n (cm^{-3})	μ (cm^2/V.s)
Cu 0 wt.%	0.87	1.31E20	54.09
Cu 1 wt.%	1.40	1.05E20	42.25
Cu 2 wt.%	1.83	9.84E19	34.78
Cu 3 wt.%	6.68	6.42E19	14.56
Cu 4 wt.%	16.97	3.09E19	11.89

Table 3 Variation of the kinetic constant with Cu contents.

Samples	K (× $10^{-3}$$min^{-1}$)
MB	3.03 ± 0.163
Cu 0 wt. %	7..82± 0.194
Cu 1 wt. %	8.58 ± 0.240
Cu 2 wt. %	7.57 ±0.264
Cu 3 wt. %	7.07 ±0.249
Cu 4 wt. %	6.82 ± 0.314

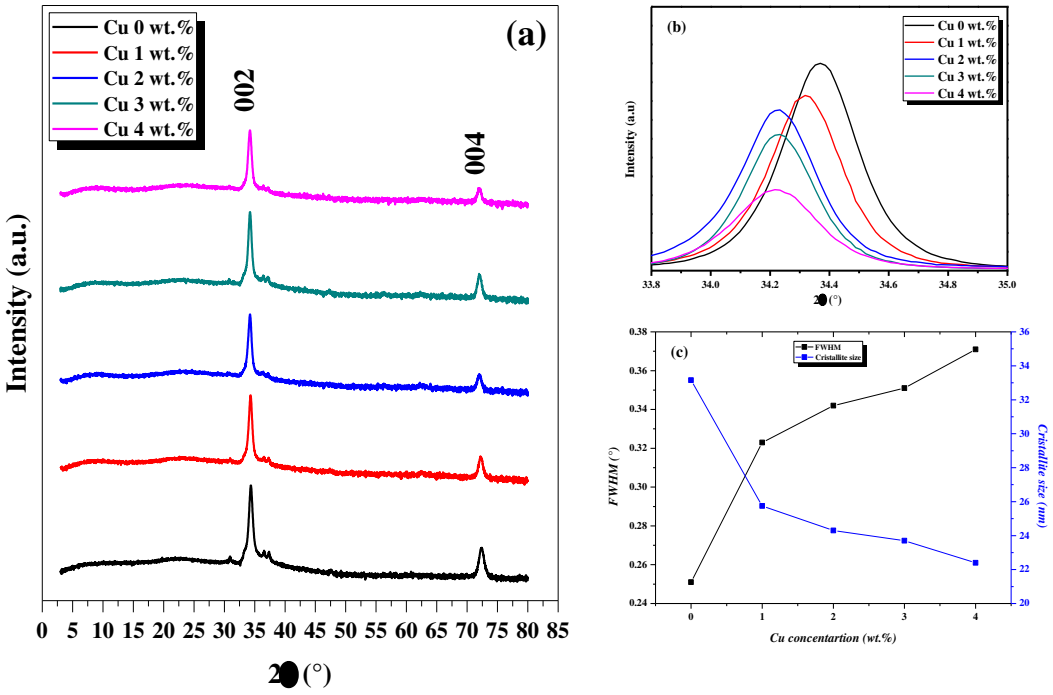

Fig. 1 X-ray diffraction (XRD) patterns of the Cu doped ZnO thin films at various Cu contents**(a)**, the enlarging XRD patterns of the (002) plane peak **(b)**, the variation of FWHM and crystalline size at various Cu contents **(c)**.

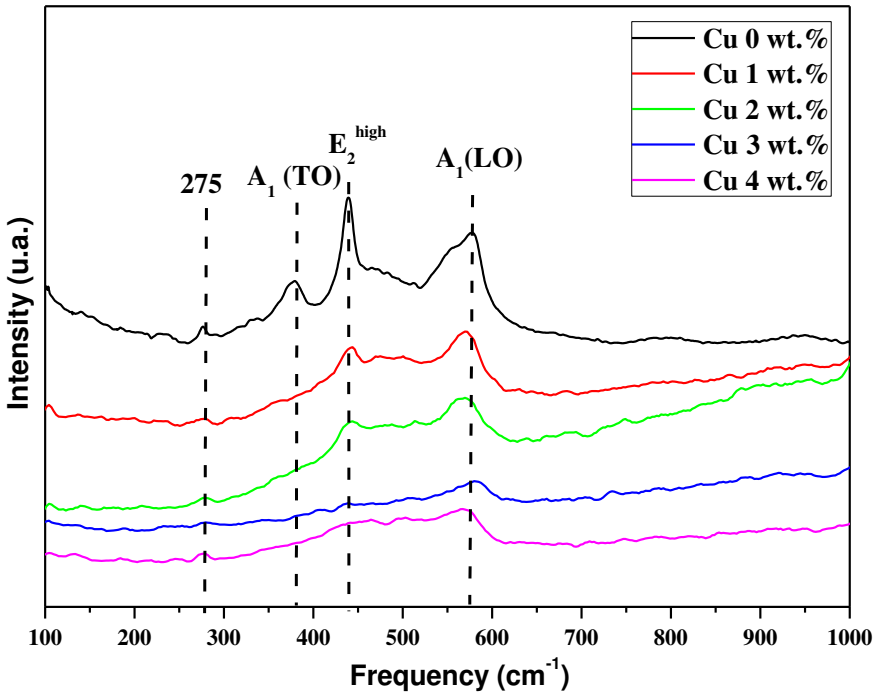

Fig. 2 Raman scattering spectra of the Cu doped ZnO films at various Cu contents

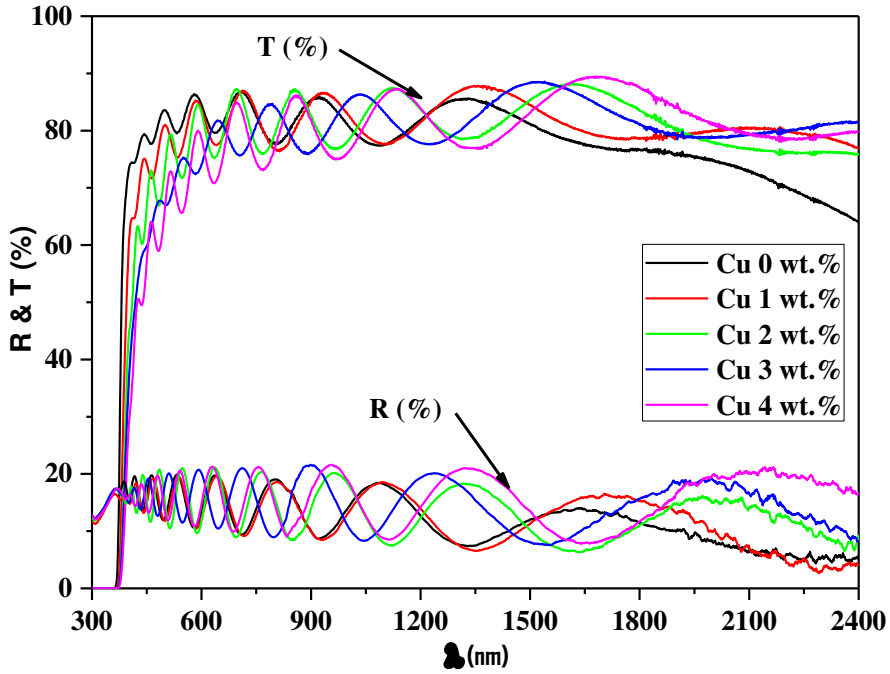

Fig. 3 Optical transmission and reflectance of Cu-doped ZnO thin films at various CuContents

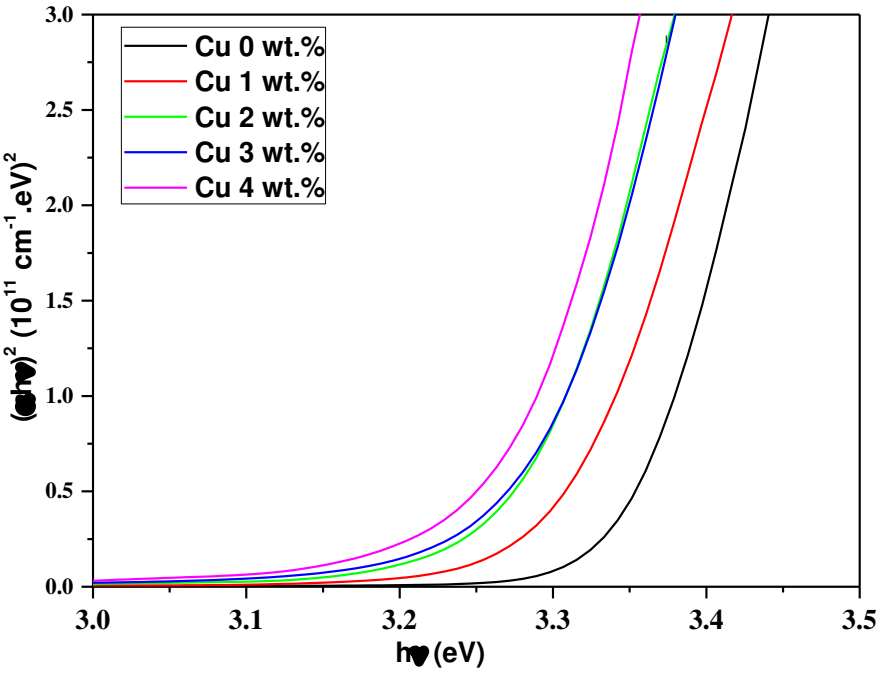

Fig. 4 The plots of *(ahv)*^{2} against *hv* of Cu-doped ZnO thin films at various Cu contents

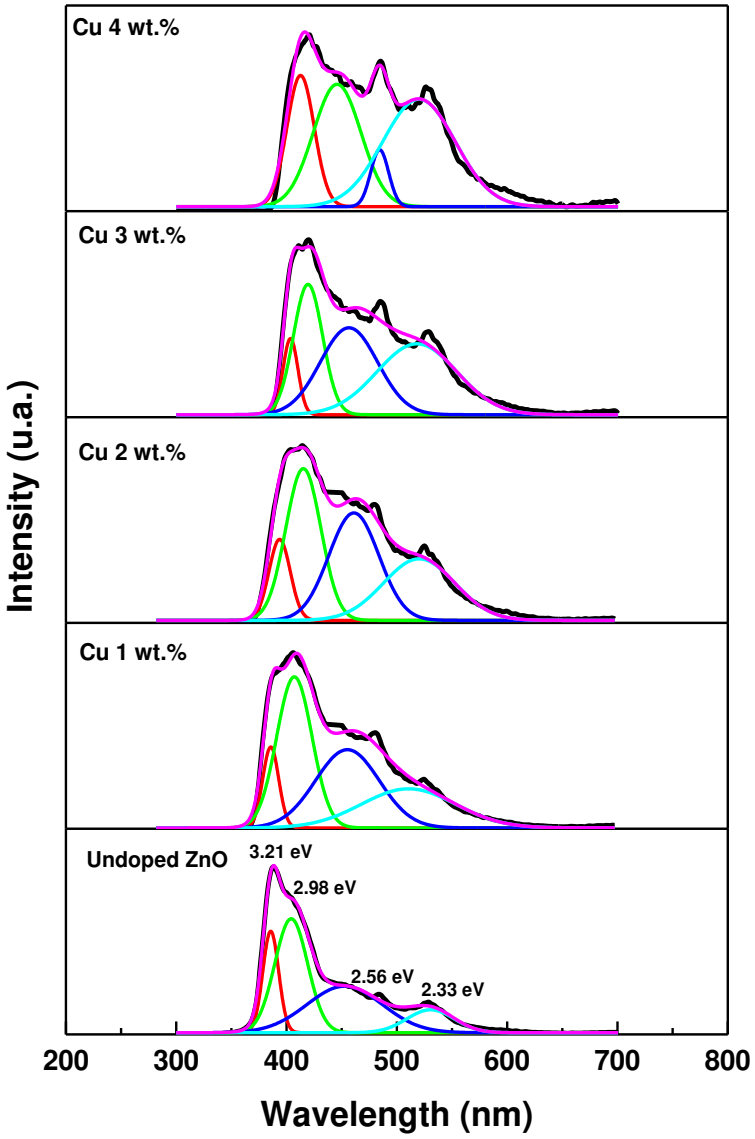

Fig. 5 Deconvoluted PL spectra of undoped and Cu-doped ZnO films at various Cu contents

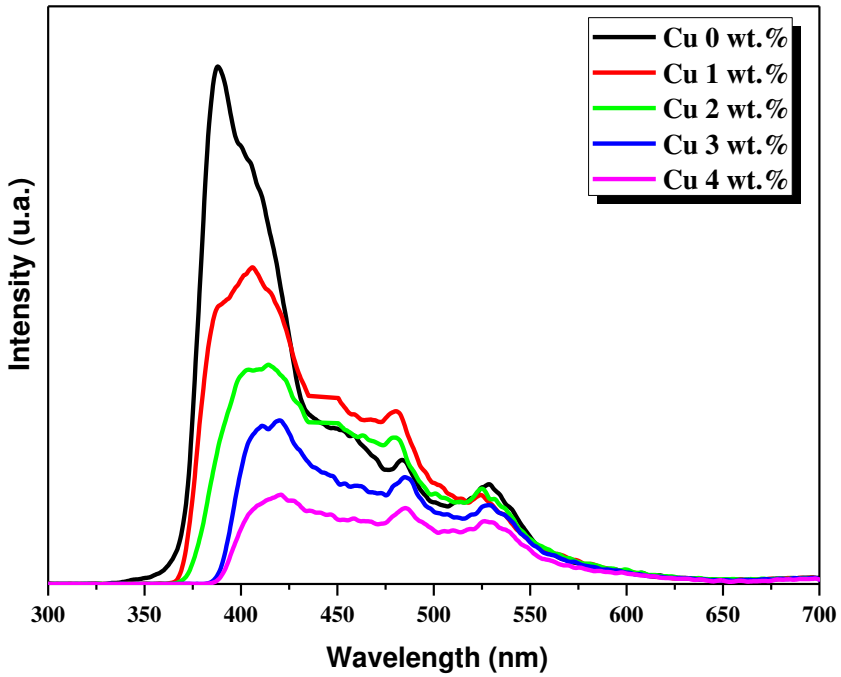

Fig. 6 PL spectra of undoped and Cu-doped ZnO films at various Cu contents

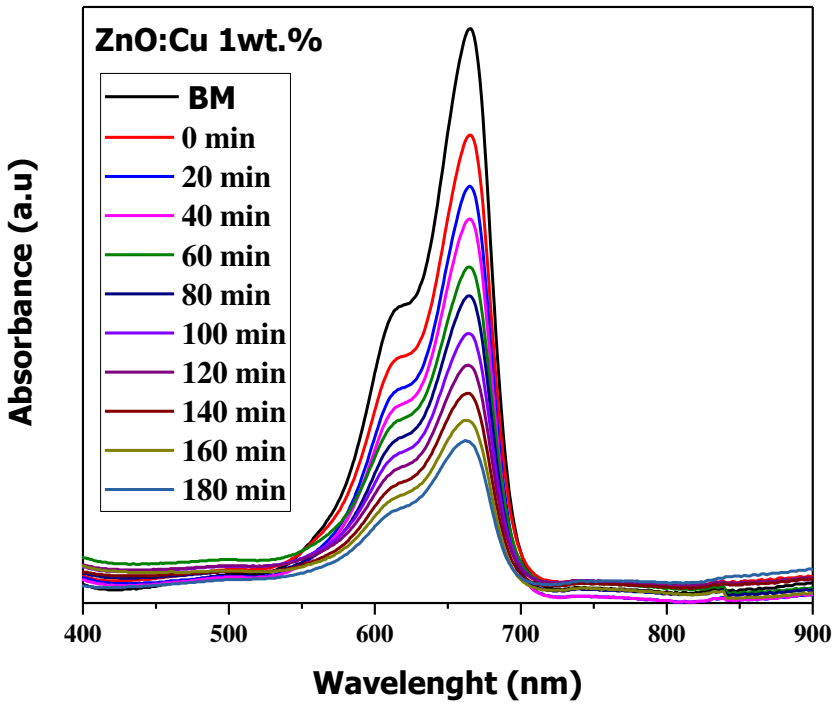

Fig. 7 The absorption spectra of MB for the 1 wt.% Cu doped ZnO film

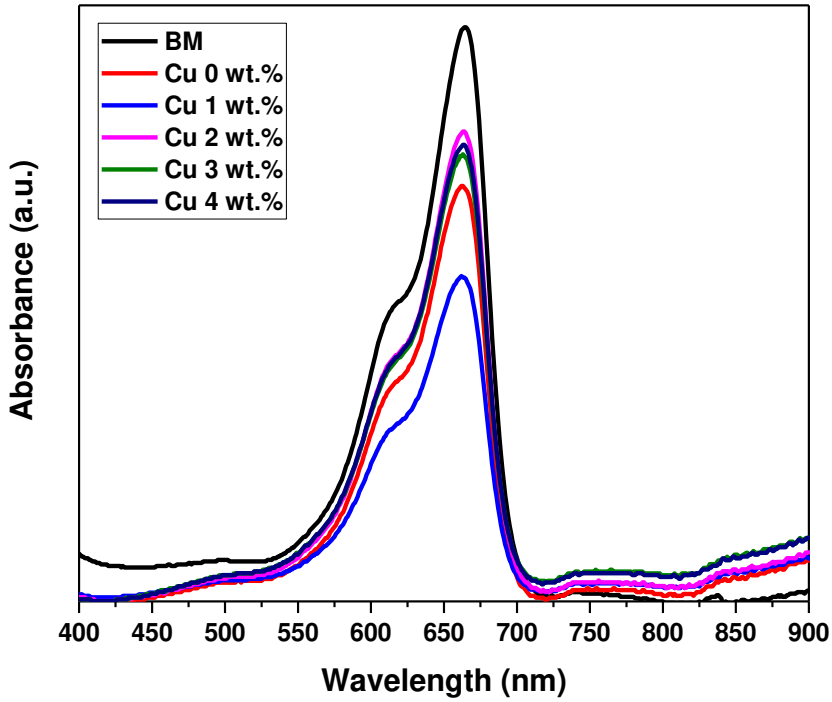

Fig. 8 Absorption spectra of MB after solar irradiation for 3 hours using the Cu doped ZnO thin films at various Cu contents.

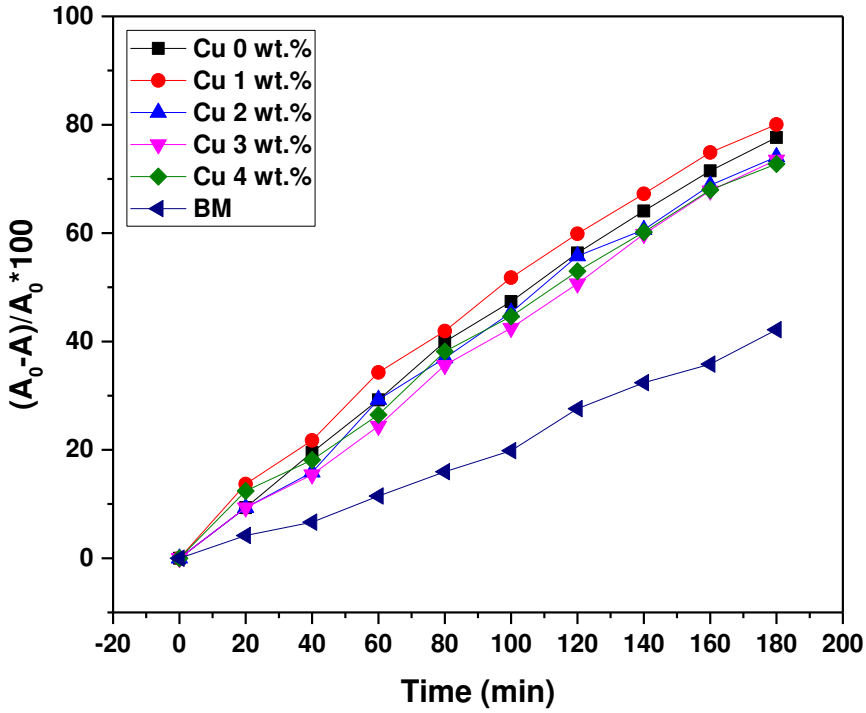

Fig 9 The degradation efficiencies of MB dye versus irradiation time

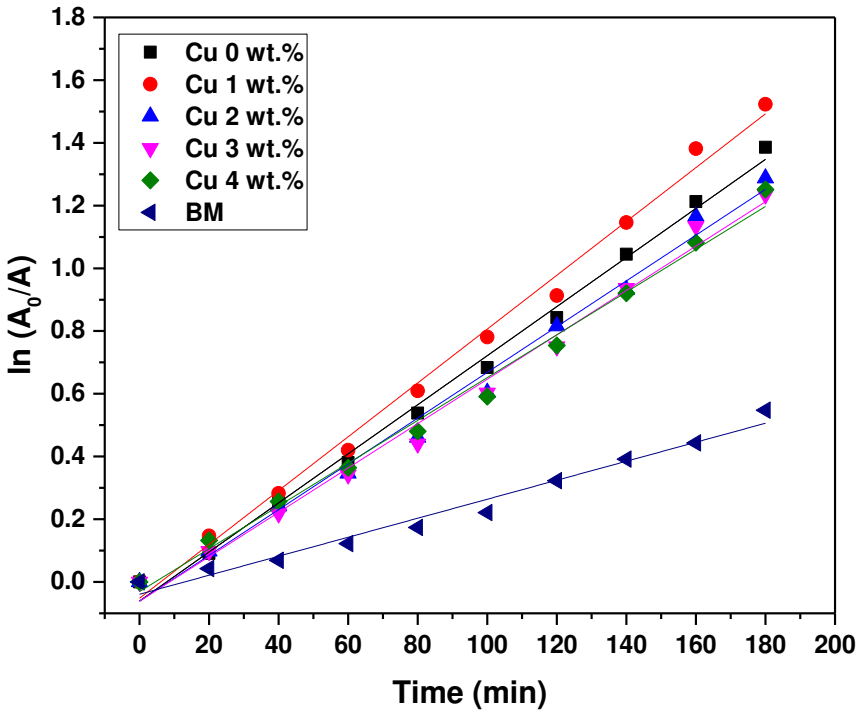

Fig. 10 Photocatalytic degradation kinetics of MB for different photocatalytic systems as a function of time under solar irradiation.

Figures

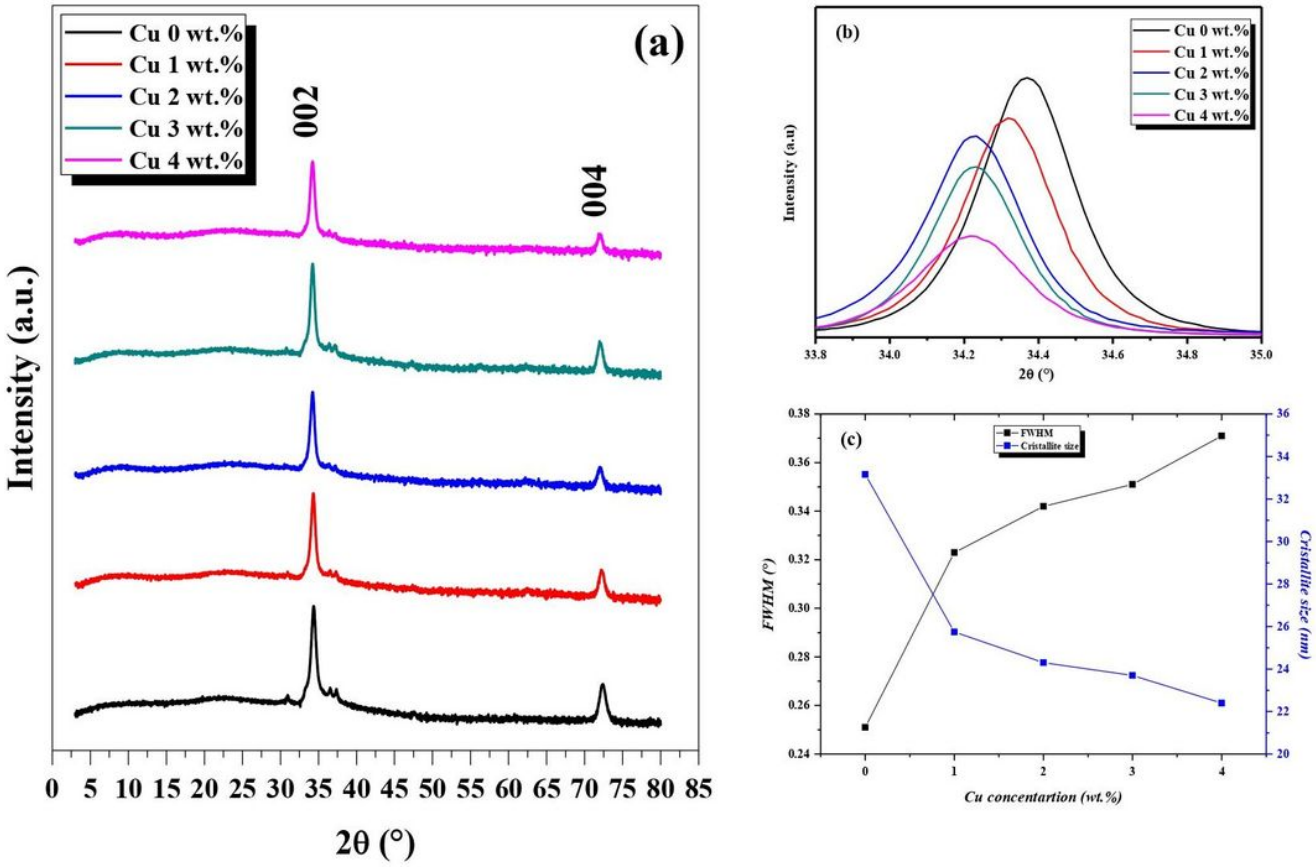

Figure 1

X-ray diffraction (XRD) patterns of the Cu doped ZnO thin films at various Cu contents(a), the enlarging XRD patterns of the (002) plane peak (b), the variation of FWHM and crystalline size at various Cu contents (c).

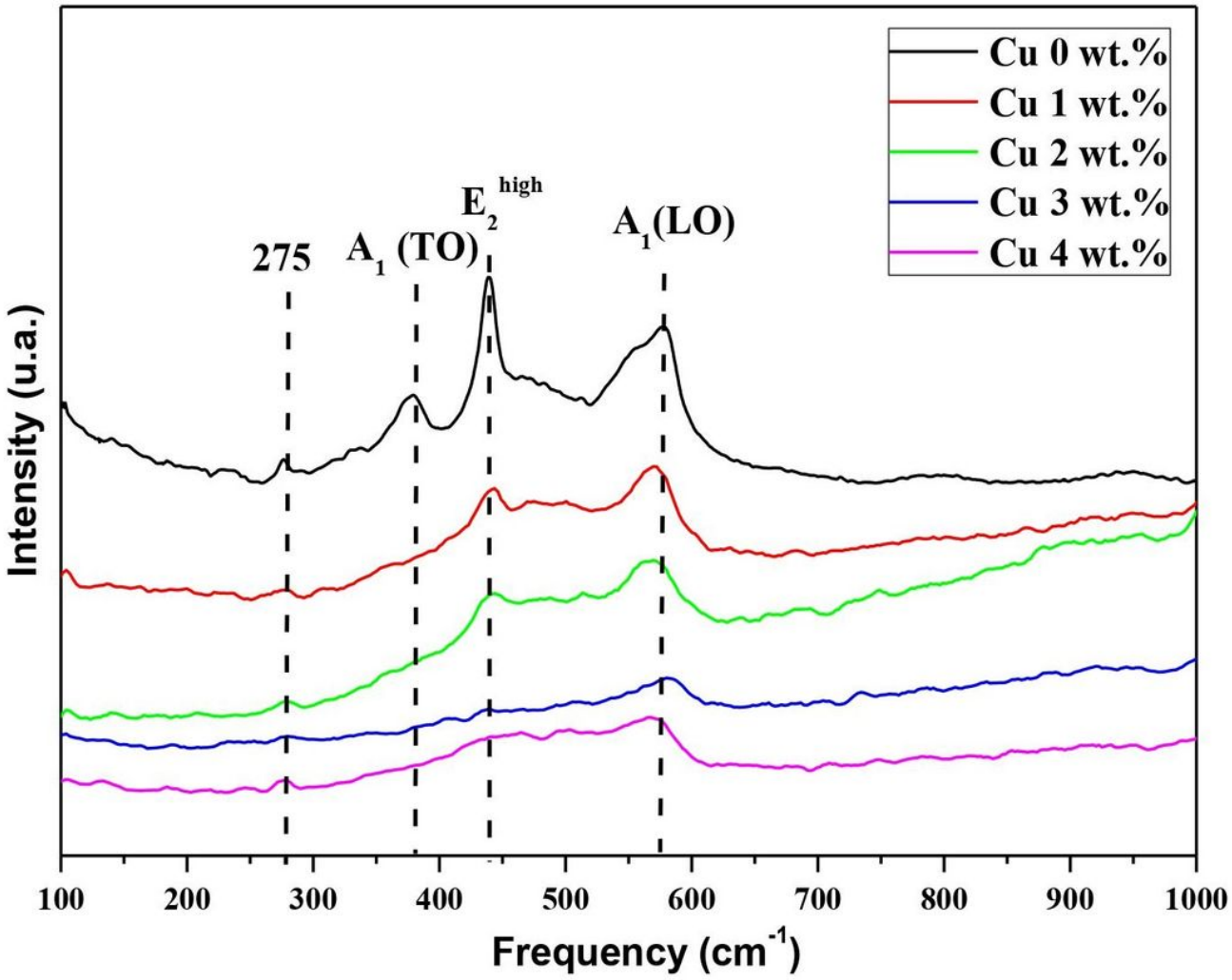

Figure 2

Raman scattering spectra of the Cu doped ZnO films at various Cu contents

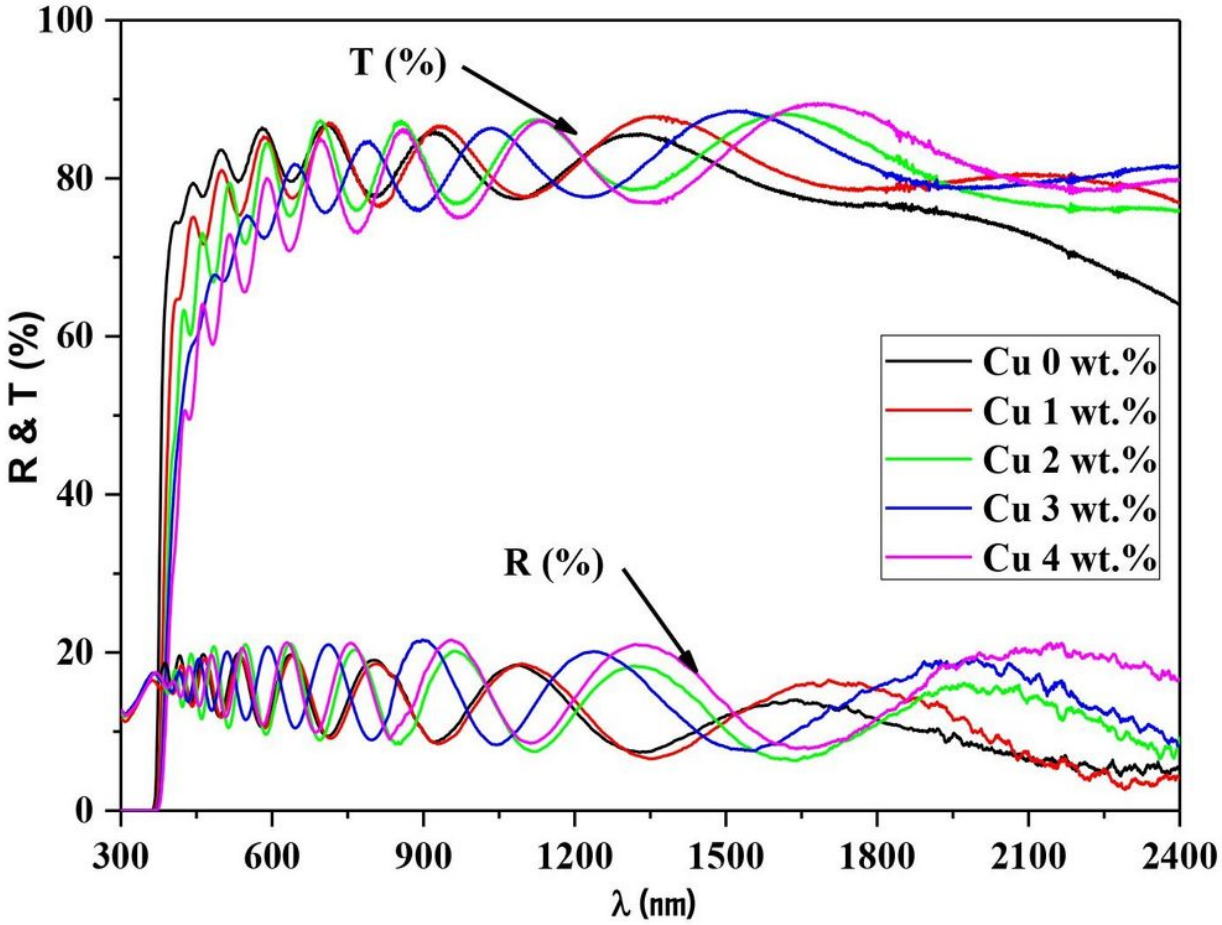

Figure 3

Optical transmission and reflectance of Cu-doped ZnO thin films at various CuContents

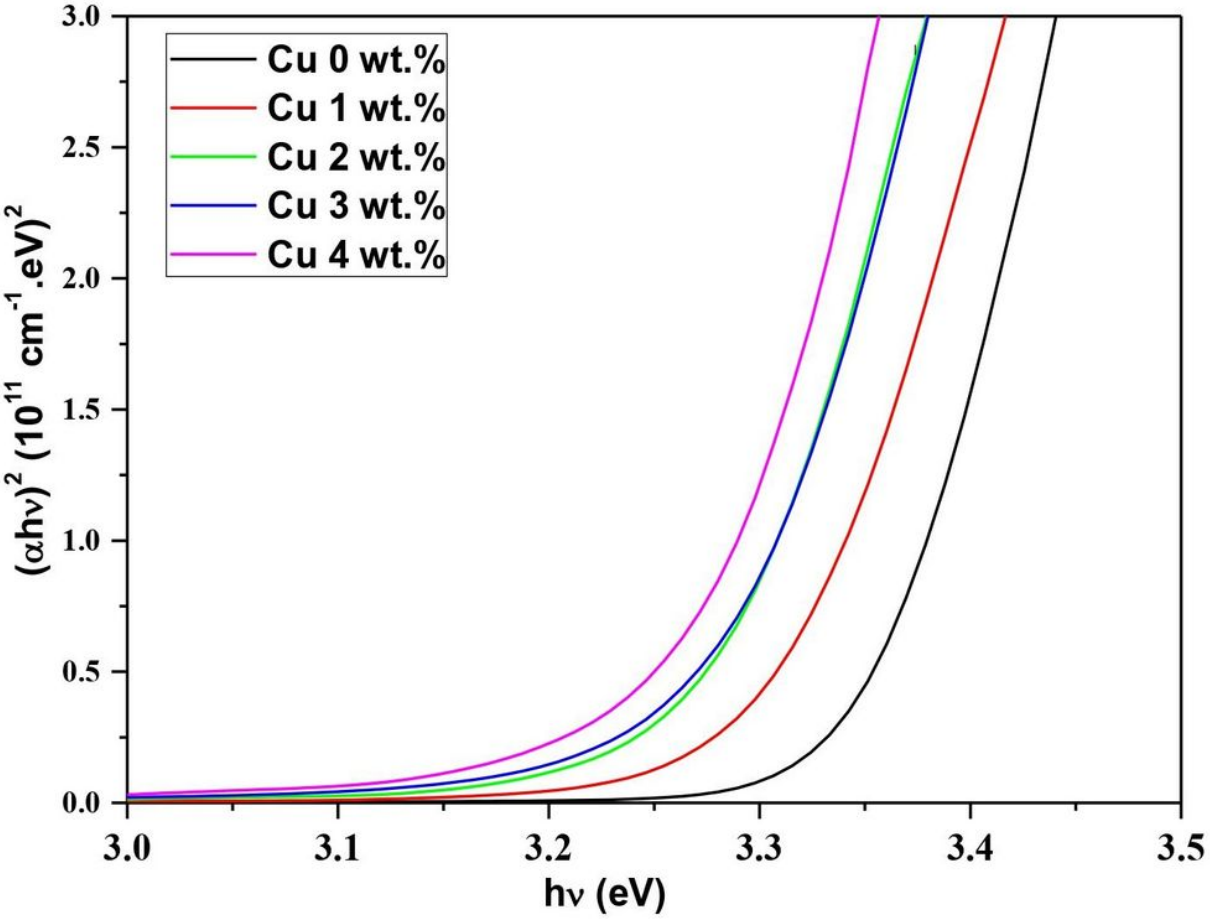

Figure 4

The plots of (ahv)2 against hv of Cu-doped ZnO thin films at various Cu contents

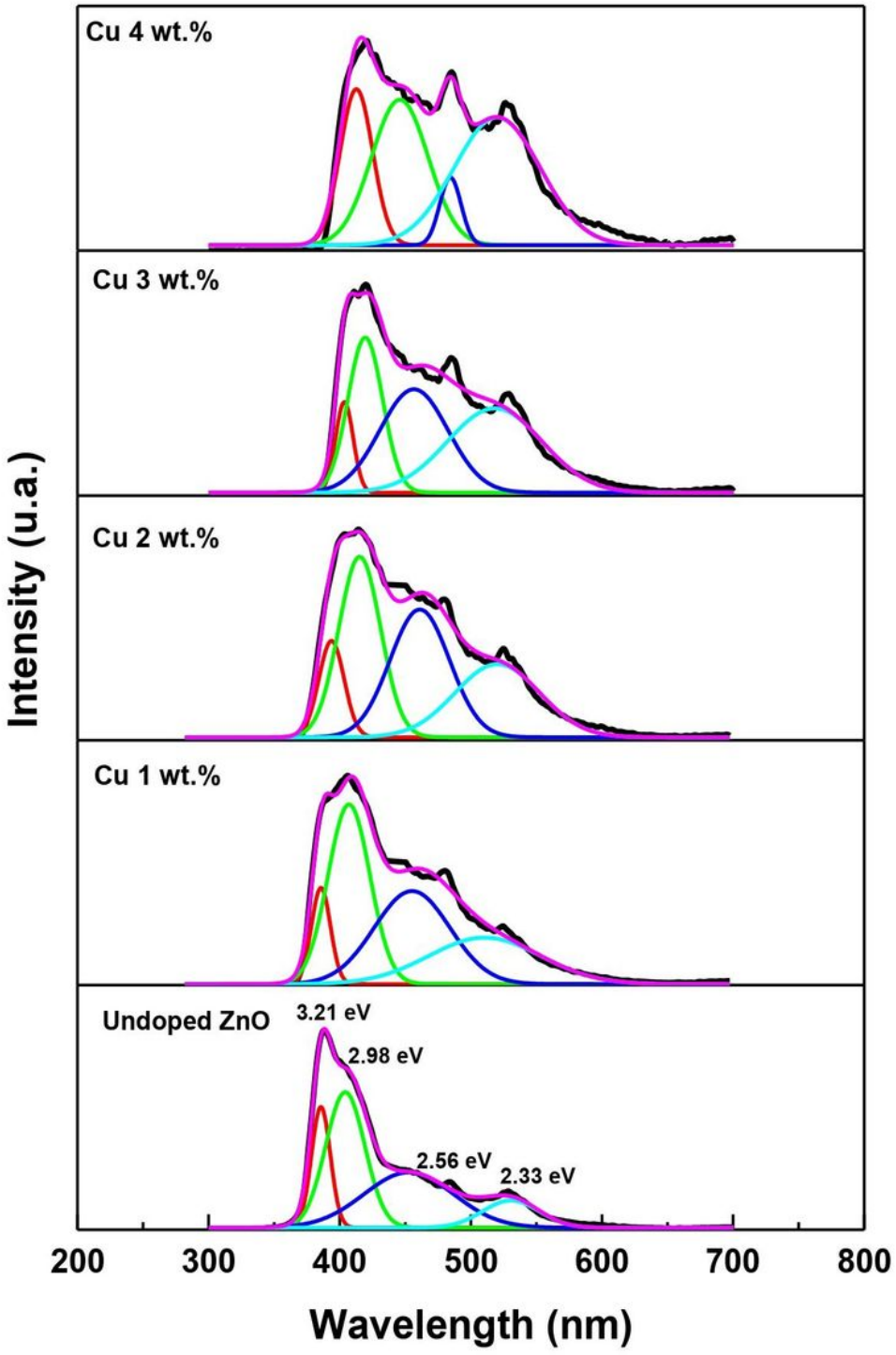

Figure 5

Deconvoluted PL spectra of undoped and Cu-doped ZnO films at various Cu contents

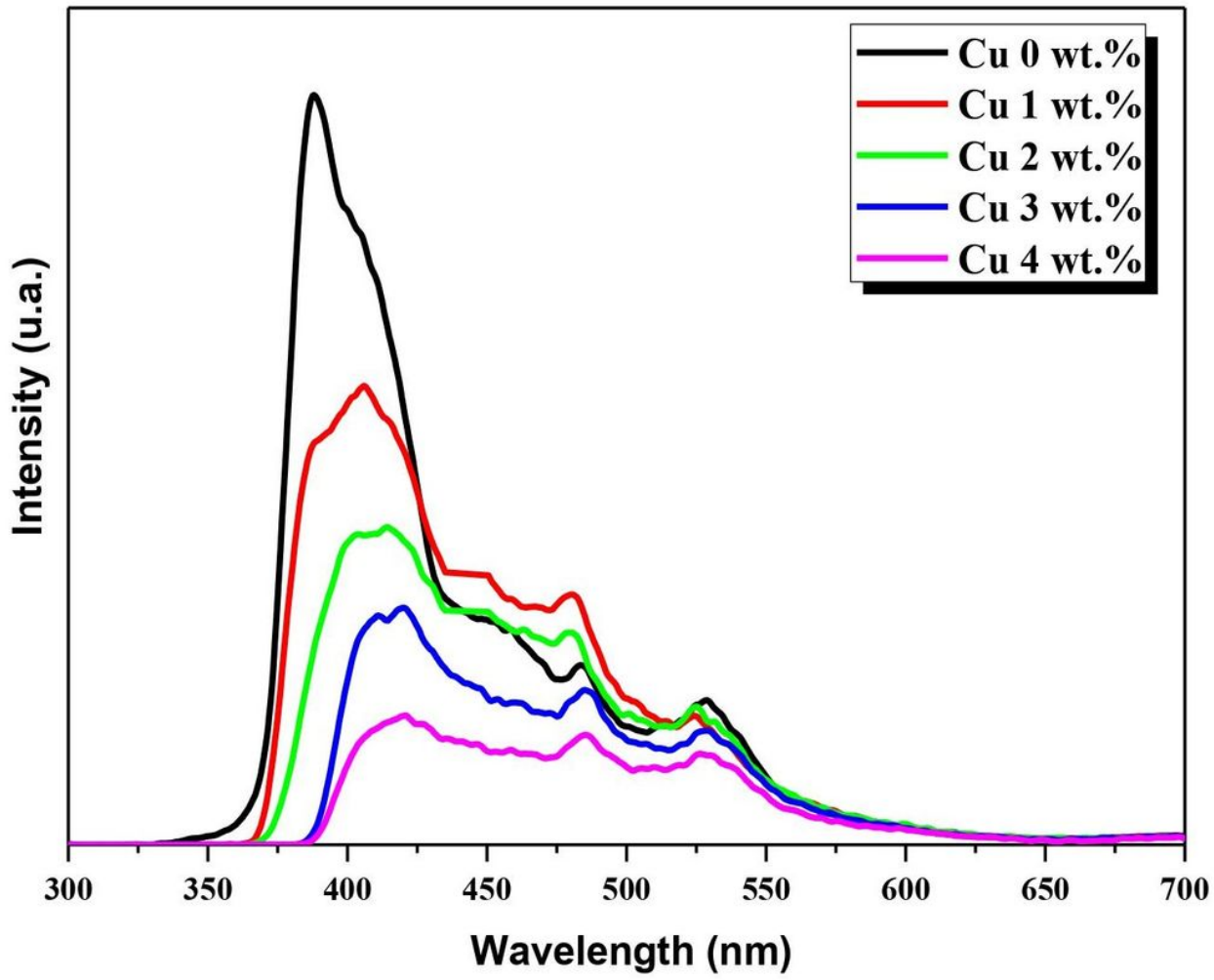

Figure 6

PL spectra of undoped and Cu-doped ZnO films at various Cu contents

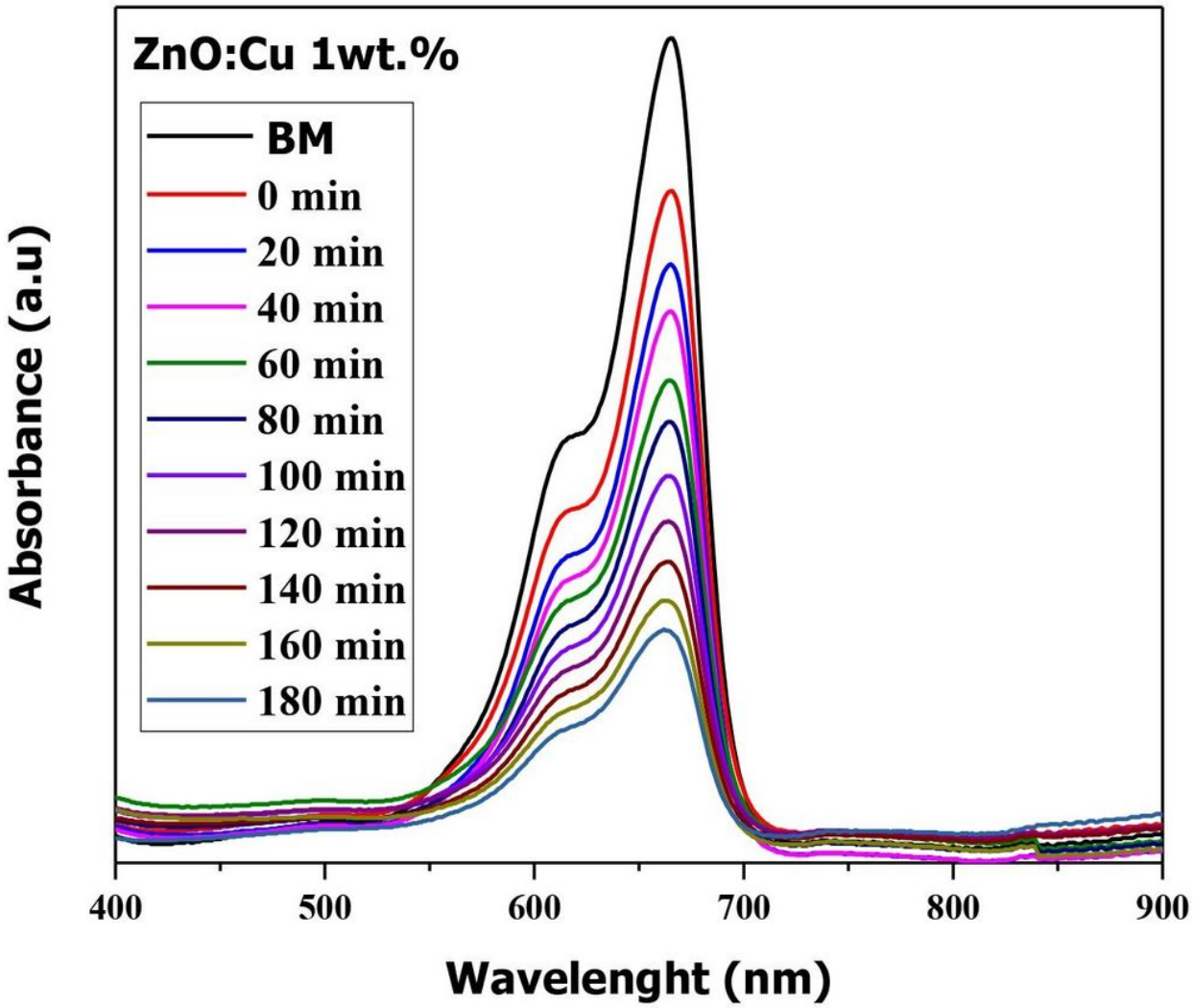

Figure 7

The absorption spectra of MB for the 1 wt.% Cu doped ZnO film

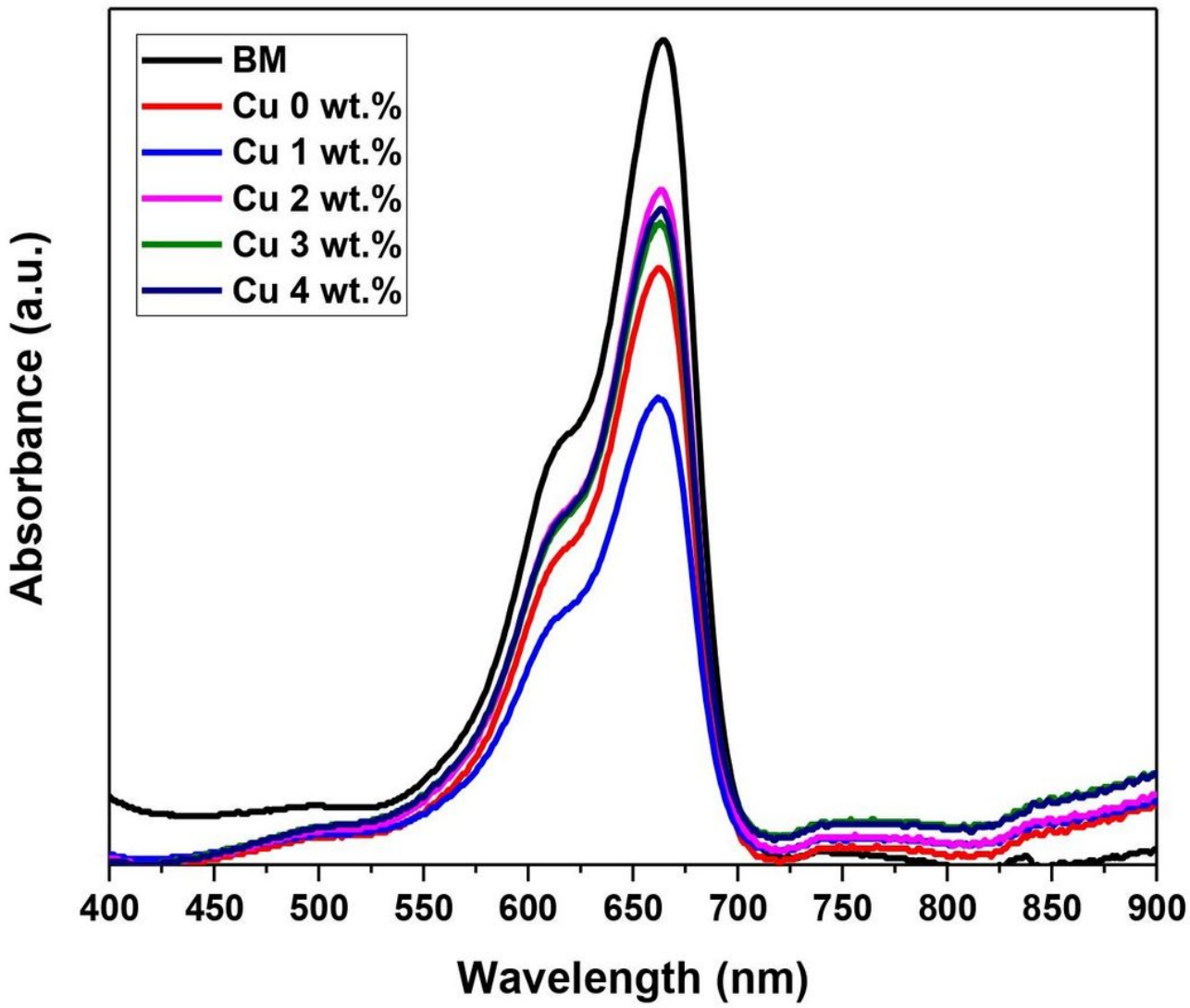

Figure 8

Absorption spectra of MB after solar irradiation for 3 hours using the Cu doped ZnO thin films at various Cu contents.

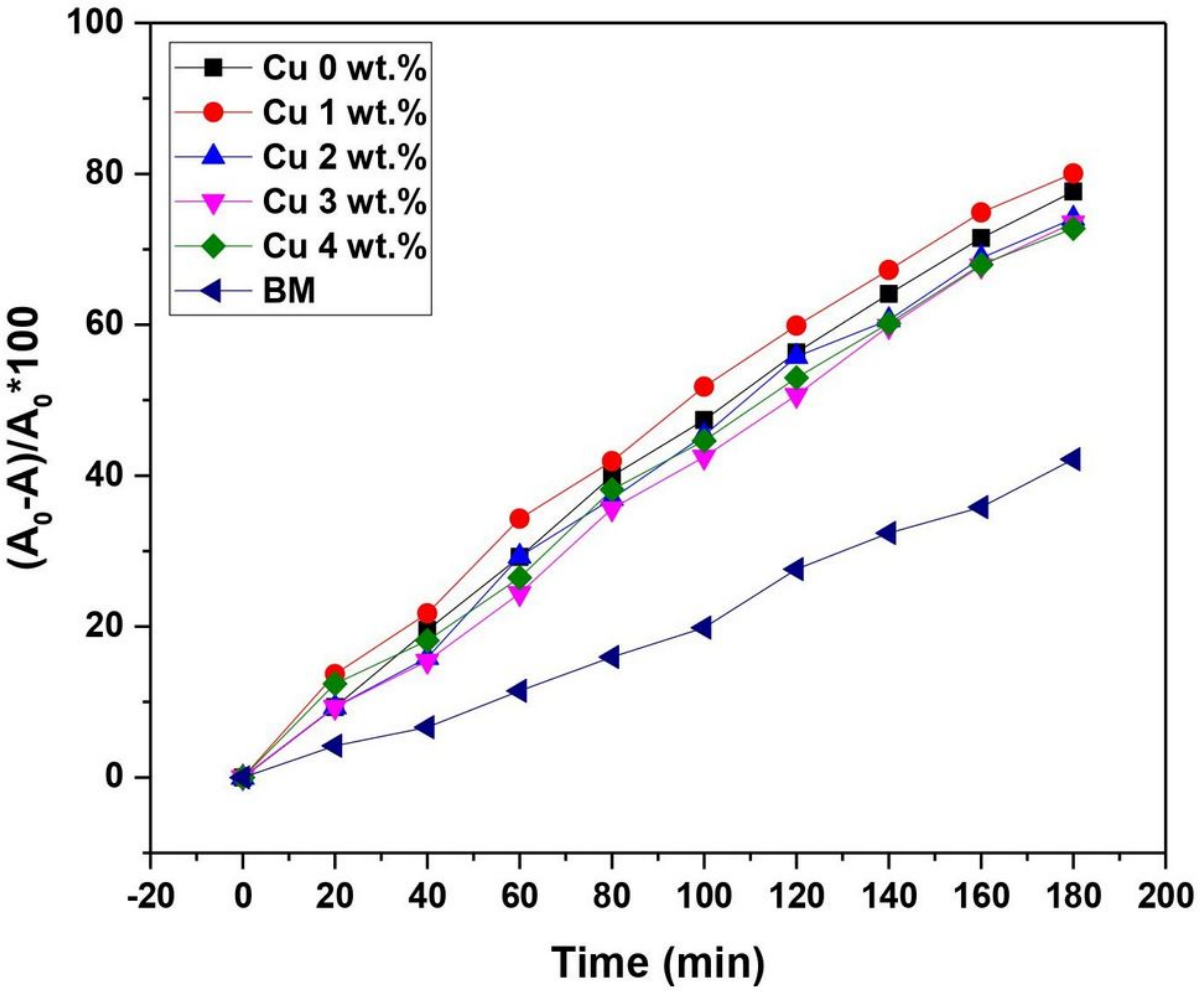

Figure 9

The degradation efficiencies of MB dye versus irradiation time

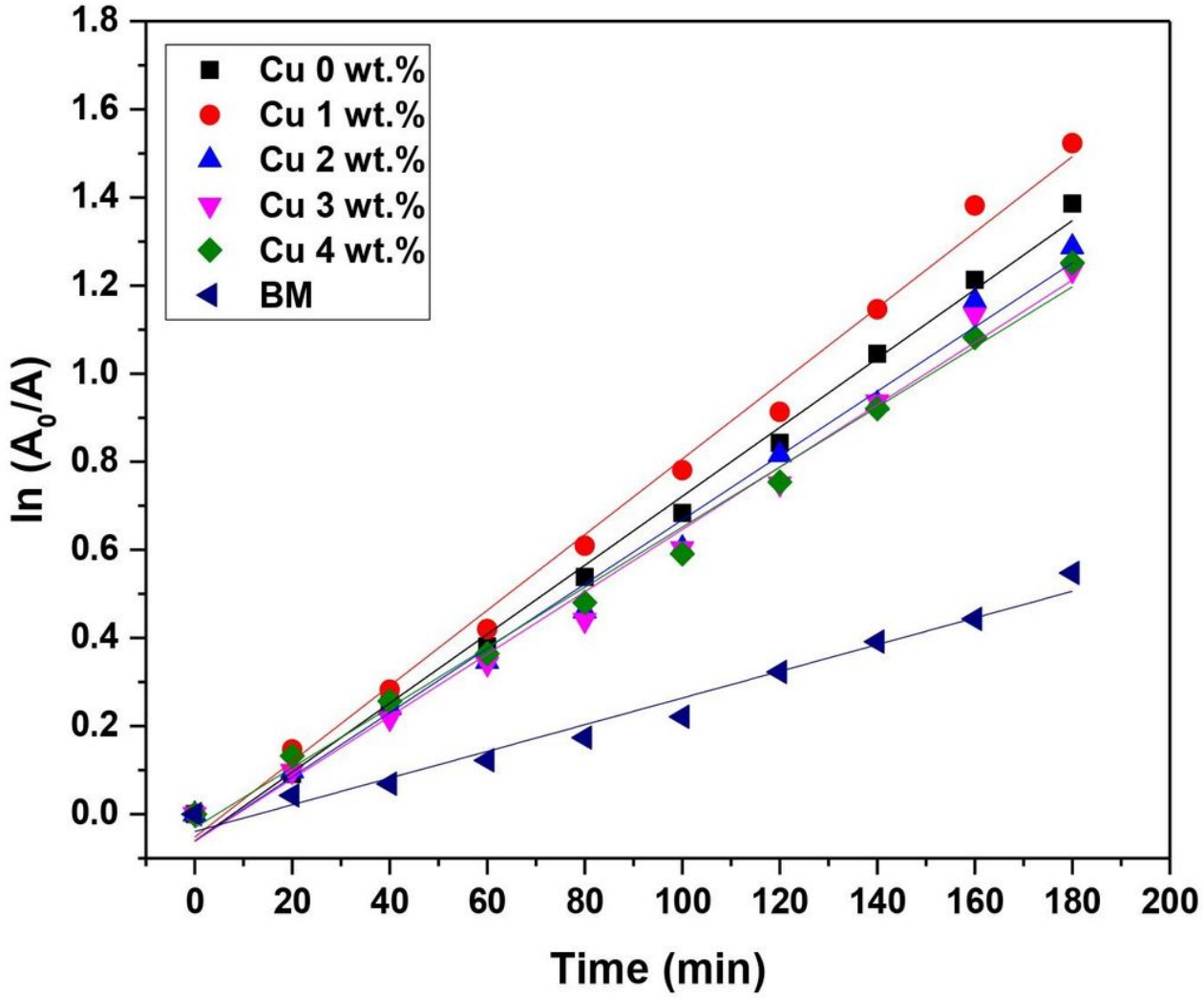

Figure 10

Photocatalytic degradation kinetics of MB for different photocatalytic systems as a function of time under solar irradiation.